Terr. Atmos. Ocean. Sci., Vol. 31, No. 6, 619-632, December 2020 doi: 10.3319/TAO.2020.04.21.01

Climatology of West Africa boundary layer

Semou Ndao[1], Andre Lenouo[2, *], Daouda Badiane[1], Michel Penka[3], Clement Tchawoua[3], Saïdou Moustapha Sall[1], and Amadou T. Gaye[1]

[1] *LPAO-SF, ESP-University Cheikh Anta Diop, Dakar, Senegal*
[2] *Department of Physics, Faculty of Science, University of Douala, Douala, Cameroon*
[3] *LEMAP, Department of Physics, Faculty of Science, University of Yaounde I, Yaounde, Cameroon*

Article history:
Received 3 October 2019
Revised 23 March 2020
Accepted 21 April 2020

Keywords:
Boundary layer height, Trends, Africa monsoon, Inter Tropical Convergence Zone

Citation:
Ndao, S., A. Lenouo, D. Badiane, M. Penka, C. Tchawoua, S. M. Sall, and A. T. Gaye, 2020: Climatology of West Africa boundary layer. Terr. Atmos. Ocean. Sci., 31, 619-632, doi: 10.3319/TAO.2020.04.21.01

ABSTRACT

Monthly means, seasonal variances, and trends of a global climatology boundary layer height (BLH) over West Africa are presented based on 36 years (1979 - 2014) of six-hourly ERA-Interim reanalysis. In this region, we found that there is a link between the West Africa Monsoon (WAM) and the monthly means of BLH where largest values of BLH variances are developed in the tropics close to the Inter Tropical Convergence Zone (ITCZ). High temperatures and sufficient moisture are also available close this area. Seasonal trend magnitudes vary from -20 to 20 m per decade during the period 1979 - 2014 and characterize by negative trend over east of the Sahara region. Trends are only included in the analysis, if their probability exceeds the 95% significance level. Case study of diurnal variation was done during the African monsoon multidisciplinary analyses Special Observing Period 3 (AMMA SOP3) experiment (August 2006). We found that the lower boundary-layer appears around 875 hPa in the monsoon layer where the wind decreases at midday in interaction through exchange processes with air originating from above the boundary layer. In the same time, the dust in Saharan Air Layer (SAL) seems to modify the atmospheric boundary layer (ABL) thermodynamic attributes by altering the shortwave and longwave radiative budget.

1. INTRODUCTION

The atmospheric boundary layer (ABL) is the part of the troposphere that is directly influenced by the presence of the earth's surface. As noted by Stull (1988), it responds to surface forcing with a timescale of about an hour or less. The energy budget exchange with surface like friction, sensible and latent heat flux or terrain induced flow modification have thus to be considered. Hence, due to variations of solar radiation, the exchanges are clearly influenced by diurnal changes. Solar radiation and atmospheric longwave radiation warm the surface and provide energy to drive weather and climate. Therefore, the boundary layer height (BLH) varies in time and space, ranging from hundreds of meters to a few kilometres. In the climatology literature, it is not common discussion of mixing height or other measures of planetary boundary layer (PBL) height (Seidel et al. 2012). Two factors can explain these reasons. Firstly, in climate models, the evaluation of PBL height in many schemes was less explicitly prescribed (Xu et al. 2015; Kang et al. 2016). Secondly, the climatologycal study of observational PBL are not fully understood, mainly because of the lack of direct measurements of PBL height particularly in the Africa region.

West Africa is found to be a unique environment where several factors influence ABL processes during the rainy season (DeLonge and Fuentes 2012). They also found that strong flows (> 10 m s^{-1}) associated with the West African Monsoon and sea breezes affect convective boundary-layer development. Farquharson (1939) found that sea to land flows dominate during the rainy season, particularly at nighttime. Onshore (sea to land) flows transport moist air, changing the inland moisture budgets and the boundary-layer thermodynamics on a daily basis (Parker et al. 2005; Schrage et al. 2007). However, Saharan Air Layer (SAL, Dunion and Velden 2004) also disturbs the diurnal growth patterns of ABL. The level of SAL is between 800 and 500 hPa (Carlson and Prospero 1972) and is located around 17°N when the wind moves westward through Sahel towards Atlantic

* *Corresponding author*
E-mail: lenouo@yahoo.fr

Ocean. A reduction of incoming solar radiation at the surface layers energy exchanges, reduces boundary-layer entrainment rates, and leads to relatively shallower mixed layers (Slingo et al. 2006). Since the work of Flamant et al. (2007), it is known that SAL events affect the ABL in West Africa and as noted by DeLonge and Fuentes (2012) there is a dearth of field observations documenting such impacts. As noted by Seidel et al. (2010), studies of the PBL have been highly localized and of relatively short duration. Hence, these authors explore some issues pertinent to the development of such a climatology, which would have applications for example in interpreting BLH obtained in nontraditional ways, such as from ground-based and space-based lidar measurements of aerosols, from boundary-layer profiler observations, from cloud base estimates from ceilometers, and from Global Navigational Satellite System radio occultation Measurements.

Seidel et al. (2010) have used daily observations of the global, land-based radiosonde station network from 1999 to 2008 obtained from the Integrated Global Radiosonde Archive (IGRA) to estimate planetary BLH. Moreover, the data were not available for a given observation time and for all four seasons. Seidel et al. (2012) have analyzed the seasonal and diurnal variations of BLH over continental United States and Europe from 1981 to 2005, with radiosonde observation, a reanalysis (ERA-Interim) that assimilates observations, and two contemporary climate models (Simulations from the NOAA Geophysical Fluid Dynamics Laboratory's Atmospheric Model 3 and from the National Center for Atmospheric Research Community Atmosphere Model version 5.0). They found that reanalysis and climate models produce deeper layers than radiosonde observations, due to difficulties in simulating stable conditions. On 505 radiosonde stations used in their study, only three were localized over West Africa. This is why, we analyzed in this work the data and surface-atmosphere BLH obtained from ERA-Interim data on the period of 36-years (1979 - 2014).

The goal of the present study is to investigate the climatology of West Africa BLH and study processes governing ABL thermodynamics and dynamics. To determine the diurnal effects of atmospheric conditions that influence the most control on the BLH, during the rainy period, we evaluated the relative importance of diurnal surface-atmosphere exchanges of energy as compared to the impacts of circulation patterns, the WAM, on BLH dynamics and thermodynamic over this region, during Africa Monsoon Multidisciplinary Analysis (AMMA) campaign SOP3 in August 2006. This study is organised as follows: in section 2, we present data and method used, the results are discussed in section 3, and conclusion is presented in section 4.

2. DATA AND METHODOLOGY

2.1 Data

We use 6-hourly ERA-Interim data during 36-years (1979 - 2014) on the latitude-longitude resolution of 0.75° × 0.75° (available at http://data.ecmwf.int/data/). Wind speed (U), specific humidity (q), virtual potential temperature (θv) and BLH were derived from ERA-Interim. Vertical cross-sections extending from 1000 to 500 hPa (every 25 hPa from 1000 to 750 hPa and every 50 hPa from 750 to 500 hPa) were used to identify heat, moisture, and wind-speed gradients from 20°W to 30°E and from equator to 30°N. The vertical extend includes the three regions on the basis of the behaviour of the basic atmospheric parameters: the surface, the free convection and the mixing layer. ERA-Interim has 60 model levels in the vertical and horizontal resolution of 0.75 degrees, which include boundary layer height estimates where the boundary layer is fairly well resolved with the lowest model levels at about 10, 30, 60, 100, 160, and 240 m above the model surface (Dee et al. 2011).

To study the vegetation of West Africa we have used dataset from the International Geosphere-Biosphere Programme (IGBP) which defines ecosystems surface classifications. The CERES (Clouds and Earth's Radiant Energy System) 10-min data can be used to derive the land categories (https://climatedataguide.ucar.edu/climate-data/ceres-igbp-land-classification).

The Global Precipitation Climatology Project (GPCP) was established by the World Climate Research Program (WCRP) to quantify the distribution of precipitation around the globe over many years. In support of this work, an international group of precipitation experts developed and produces the GPCP version 2 monthly Satellite-Gauge (SG), which associated precipitation error estimates and covers the period January 1979 to the present, with a delay of two to three months for data reception and processing (Adler et al. 2003), Pentad which provides precipitation estimates on a 2.5-degree grid over the entire globe at 5-day (pentad) intervals for the period January 1979 to present (Xie et al. 2003), and One-Degree Daily (1DD) which provides precipitation estimates on a 1-degree grid over the entire globe at 1-day (daily) for the period October 1979 to present (Huffman 2001), combined precipitation data sets. A backup FTP site for the version 2 and 1DD products is located at NASA Goddard Space Flight Center (GSFC). Version 2 supersedes all previous versions of the GPCP monthly product. All three precipitation products are produced by optimally merging estimates computed from microwave, infrared, and sounder data observed by the international constellation of precipitation-related satellites, and precipitation gauge analyses. The precipitation gauge analysis used in the GPCP satellite-Gauge is used into study monthly variation of the climate over West Africa during 1979 - 2014.

Seven different methods are usually used to estimate BLH from radiosonde (Seidel et al. 2010). Four methods are traditional approaches often encountered in the PBL literature. They include (i) the parcel method, (ii) the level of the maximum vertical gradient of potential temperature,

(iii) the base of an elevated temperature inversion, (iv) the top of a surface-based inversion, and by using Global Navigational Satellite System radio occultation data, which can be used to derive vertical profiles of atmospheric (v) refractivity, (vi) temperature, and (vii) specific humidity. Table 1 summary these seven different methods. Figure 1 shows the values of BLH calculated from radiosonde during 2006 in different towns over West Africa using six methods. At Ouagadougou (12°12N; 1°3W), the value of BLH which are calculated from the refractivity method are under estimate whereas the surface-based inversion method over estimate. The same tendency can be found in Parakou (9°21N; 2°37E) and Tambacounda (13°18N; 12°49W). At Cotonou (6°22N; 2°26E), the six methods give (Fig. 1a) the values of BLH around 2000 m. Since radiosonde data are not regular in space and time, to study the climatology of BLH over West Africa, we will use the reanalysis data. In ECMWF ERA Interim, BLH is defined through Troen and Mahrt parcel lifting method (Troen and Mahrt 1986), and BLH data from ERA Interim is used in this work, near to values obtained from the refractivity method. We found that the Yule-Kendall index is near zero for ERA Interim data which show that these data are symmetric.

2.2 Methods

The concept of virtual potential temperature (θv in K) given in function of specific humidity (q in g kg^{-1}) by the Eq. (1) is used to determine the height of the boundary layer.

$$\theta v = \theta(1 + 0.62q) \tag{1}$$

where q is the moisture and θ the potential temperature given by

$$\theta = T(P_0/P)^{R/Cp} \tag{2}$$

Where P is the pressure (in hPa), T the air temperature (in K), R = 287.05 J K^{-1} is the specific gas constant, Cp = 1005 J kg^{-1} K^{-1} as specific heat capacity of air at constant pressure and P_0 = 1000 hPa a reference pressure. Therefore, the relative humidity can be written as

$$\varphi = \frac{q}{Q} \times 100 \tag{3}$$

while Q is the specific humidity of a saturated air at the observed temperature and pressure.

It can be approximated as

$$Q = 0.622 \times E/(P - 0.378 \times E) \tag{4}$$

with E as the saturated water vapour pressure (in hPa), calculated in function of T (in °C) as (Bolton 1980; Lenouo et al. 2008):

$$E = 6.112 \times Exp[17.67 \times T/(243.5 + T)] \tag{5}$$

Local seasonal trends in BLH are analyzed by calculate the areal weighted seasonal mean for BLH each year and use regression coefficient to calculate the trends, which performs simple linear regression on multi-dimensional arrays. The linear trend model, also known as a trend-line model is another possibility is that the local mean is increasing gradually over time. Trends are only included in the analysis, if their probability exceeds the 95% significance level. If 95% confidence intervals for two seasonal means are calculated (approximately) by adding or subtracting two standard errors, the intervals do not overlap, so the difference in means is statistically very significant. The magnitude of a given trend is estimated by linear regression, although the error is rarely normally distributed in BLH (Meukaleuni et al. 2016). For more discussion of the linear trend model, see Nau 2014. We also look for other statistical analyses as the standard error of the mean (SEM) which can be expressed as:

$$SEM = \frac{\sigma}{\sqrt{n}} \tag{6}$$

where σ is the standard deviation and n is the number of values of BLH during August 2006, and considered the root-mean-square deviation (RMSD) for the saisonnal variance.

3. RESULTS AND DISCUSSIONS

3.1 Climatology and Trends of BLH

Before examining the correlation between BLH and the precipitation, we present the map of vegetation in West Africa as represented in Fig. 2. CERES land classification from IGBPa_1198.map.nc. Surface types 1 - 17 correspond to those defined by IGBP (International Geosphere Biosphere Programme). The last 3 surface types were defined for CERES. Surface type 18, Tundra; fresh snow, number 19, and sea ice, number 20 are not permanent surface types. They are obtained daily from the National Snow and Ice Data Center. The IGBP surface type for Sahara is 16, for the Sahel zone is 1 and the Congo basin, which is dense forest in Central Africa to 4. This figure also shows the four radiosondes sites over West Africa: Cotonou, Ouagadougou, Parakou, Tambacounda.

The distribution of monthly means of BLH (1979 - 2014) is displayed in Fig. 3. These figures show the influence of the SAL on the BLH and the impact of monsoon. The dry region of SAL corresponds to high values of BLH over West Africa from May to September. Hence in the rainy season,

Table 1. The seven methods used to derive BLH.

Method (Symbol)	Description	Reference
Parcel (par)	Height of the mixing layer is based on the vertical displacement of the air parcel on the surface. It corresponds to the height of the value of the virtual potential temperature at the value of the surface.	Holzworth 1964; Seibert et al. 2000
Maximum vertical gradient of potential temperature (Th)	The height corresponding to the maximum of the vertical gradient of the potential temperature	Oke 1988; Stull 1988; Sorbjan 1989; Garratt 1992
Specific humidity (Sh)	The height corresponding to the minimum of the vertical gradient of the specific humidity	Ao et al. 2009
Surface-based inversion (Rh)	The height corresponding to the minimum of the relative humidity	Sokolovskiy et al. 2006; Basha and Ratnam 2009
Refractivity (N)	The height corresponding to the minimum of refractivity	Smith and Weintraub 1953
Inversion of the temperature in altitude (temp)	Basis of altitude inversion of the temperature	Bradley et al. 1993
Inversion of the surface temperature	Top of the surface temperature inversion	Bradley et al. 1993

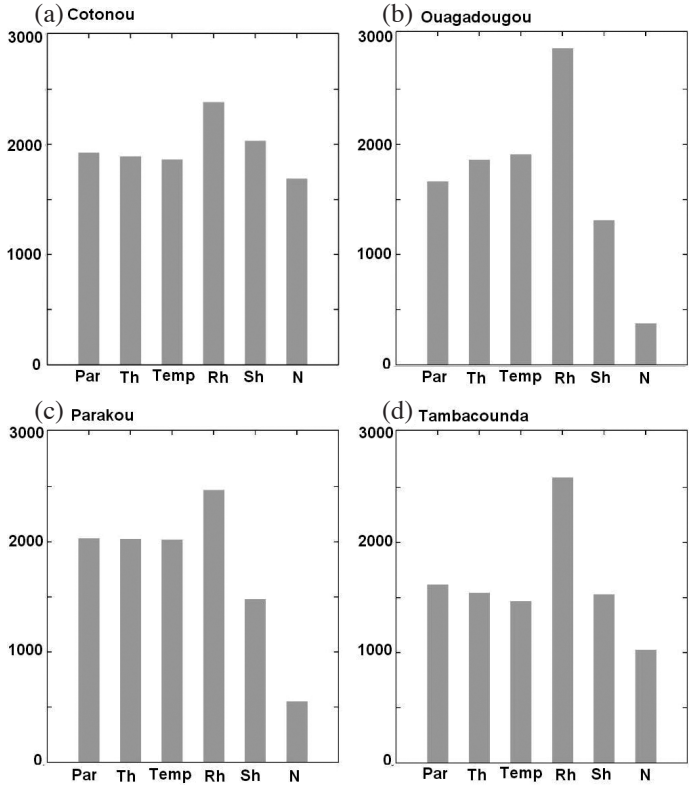

Fig. 1. Values of BLH (in meters) calculated from radiosonde during 2006 in different towns over West Africa using six methods: parcel (Par); maximum vertical gradient of potential temperature (Th); temperature inversion (Temp); surface-based inversion (Rh), specific humidity (Sh), and refractivity (N).

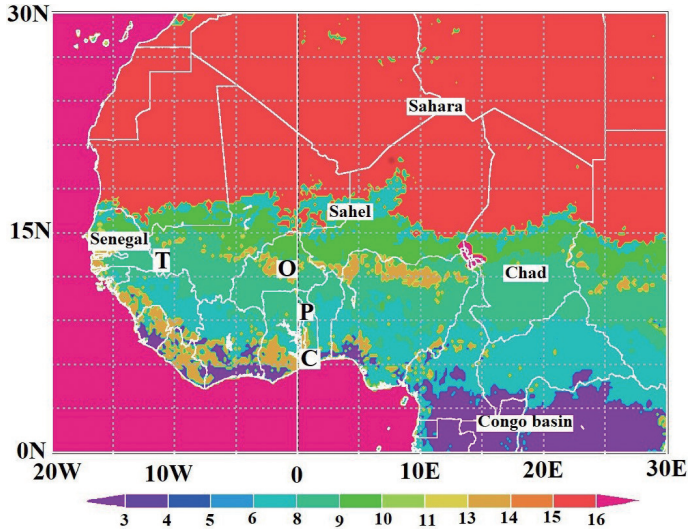

Fig. 2. Map the vegetation of West Africa showing the four analysis regions defined in the texte. The position of the four towns Ouagadoudou (O), Cotonou (C), Parakou (P), and Tambakounda (T) are also marked. Surface types 1 - 17 correspond to those defined in the texte.

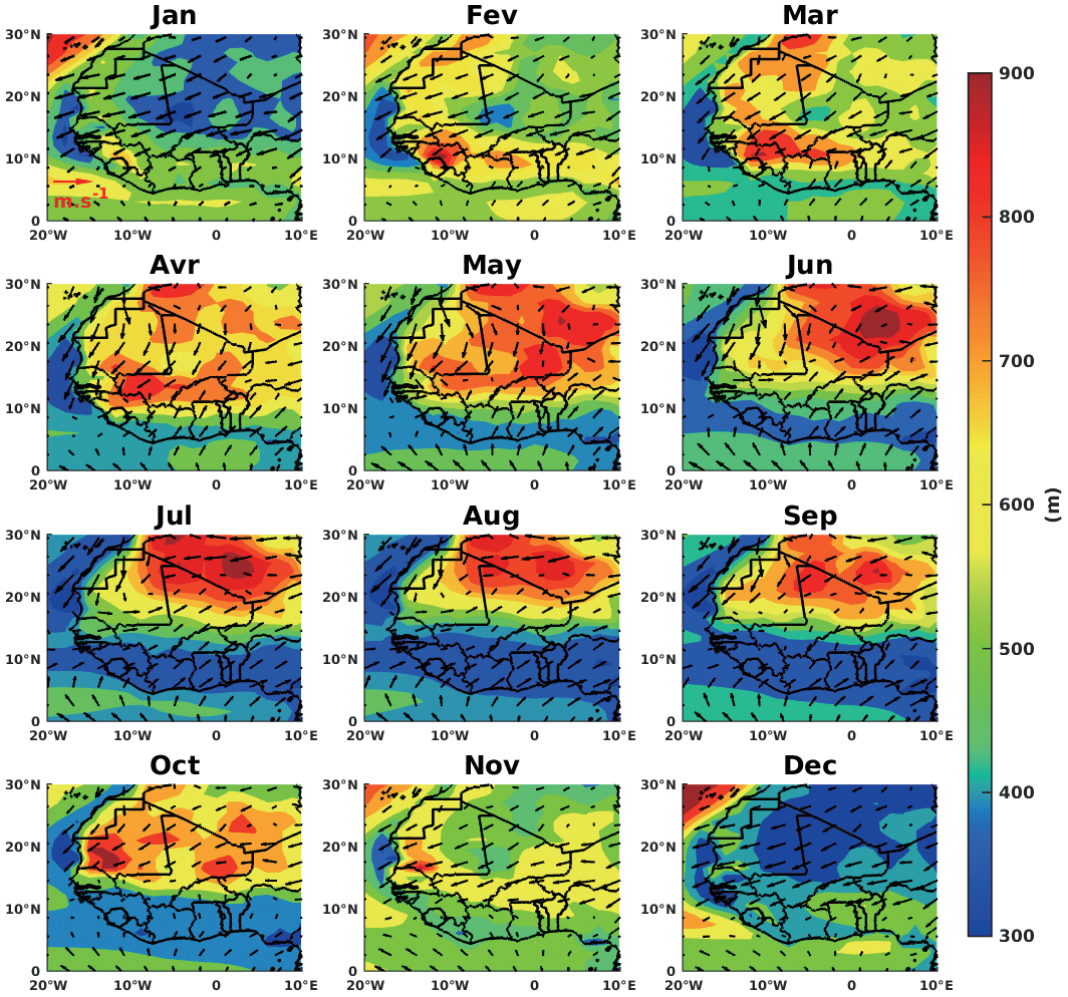

Fig. 3. Climatological (1979 - 2014) monthly means of BLH (in m) and 950 hPa wind over West Africa. BLH is in the color interval of 50 m whereas the wind vector in arrow as indicated by the legend. ITCZ appear in the month of July to September around 10 - 15°N.

the cool air from the Ocean decreases the BLH in the coastal region in opposite of the dry air from Sahel which is characterized by high values of BLH. This value is around 900 m, corresponding of the level of around 950 hPa. During the summer period (June to September), low values are located between the Equator and the monsoon front (around 15°). As evidence of the influence of the monsoon, the monthly variation of Inter Topical Convergent Zone (ITCZ) evolves during the year between dry and wet region. The ITCZ is strongly perturbed by the convective system over this region (Flamant et al. 2007). This evolution of the monsoon, gives by 950 hPa wind, shows that the monsoon arrives in the West Africa at April from south to the north before move in the north to the south at September. It is found in Fig. 2, between latitudes 9° and 24°N, the alternation of the south-westerly wind from the ocean and the harmattan from Sahara region at the surface. West African monsoon is defined by this alternation where north-easterlies occur constantly farther north, but only south-westerlies occur farther south during the rainy season (June to September). This figure also shows that the drought becomes shorter and less complete farther south. Hence, at 12°N about half the year, and at 8°N it disappears completely at the rainy season. In this region, the drought results from the arrival of dry surface air issuing from anticyclones formed beyond the Equator in the Southern Hemisphere (Flamant et al. 2007).

Figure 4 present monthly means of variations of precipitation in space, ranging from the equator to 30°N and

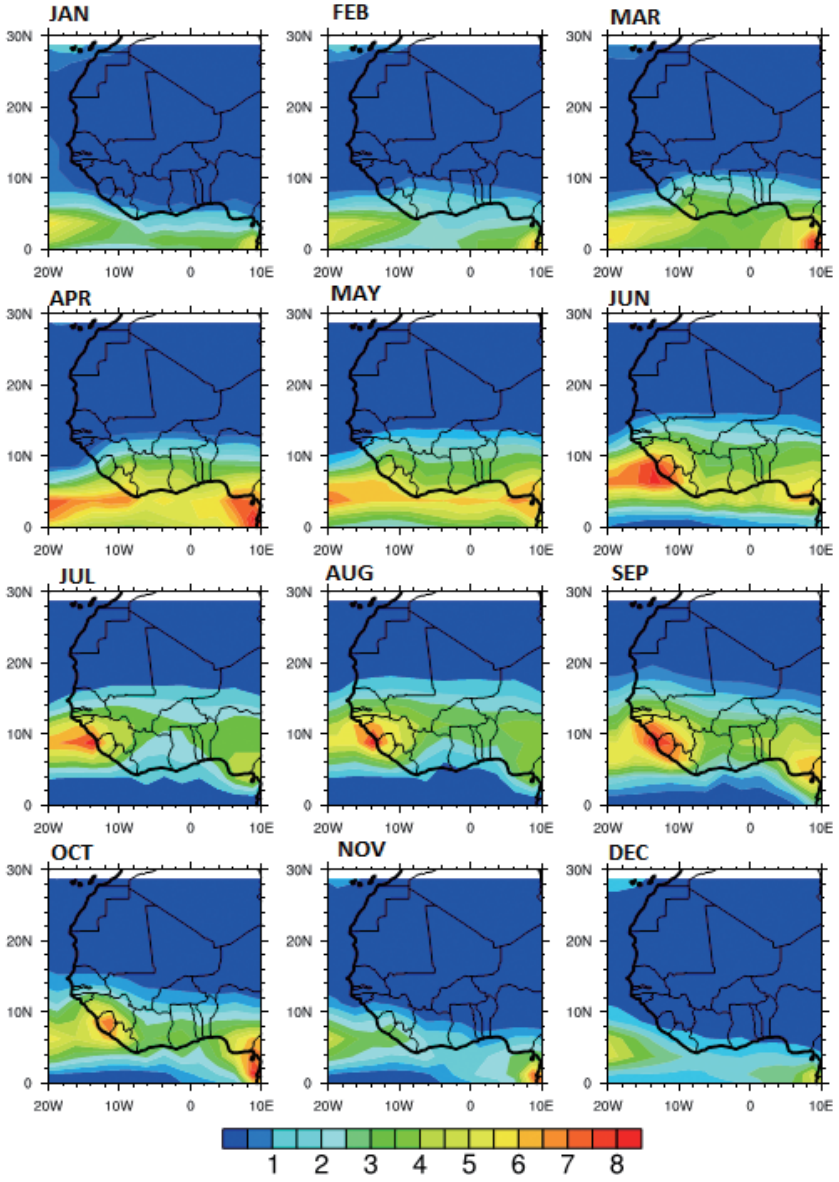

Fig. 4. Climatological (1979 - 2014) monthly means of precipitation over West Africa from GPCP reanalysis where the country contours are represented by a dash. The interval of precipitation is 1 mm day^{-1}.

covering 20°W - 10°E during 1979 - 2014. From these graphs, there is a maximum of precipitation in June over West Africa equatorial coast. This maximum moves much more northward to set around the Sahara area during the months of July and August. In September, there is maximum precipitation extends almost from the Equator to 15°N and all this confined in the band (0° - 15°N, 10°E - 15°W). Figure 4 also shows that during the spring/summer, precipitation migrates from the Guinea coast to the Sahel and back again, resulting in two rainy seasons per year in the south (April to June and August to October) and one in the north (July to September). The exchange of energy between the ocean and the surface of the continent allow creating and maintaining the lowland flow monsoon of southwest, which advects relatively cool moist air from the Gulf of Guinea onto the hot dry continent (Seidel et al. 2012).

To well understand the physical processes related to BHL, Figs. 5 - 7 show the climatology of the potential temperature at 950 hPa, the specific humidity ay 950 hPa and the vertical motion at 500 hPa with 950 hPa wind vector at 950 hPa. Hence, the Fig. 5 shows that the potential temperature is maximun during the rainy season in the dry zone of Sahara. These maximums zone also correspond to maximum BLH during this period. The meridional division of this region can be noted in the specific humidity map (Fig. 6) where four zones are clearly appear. The dry zone characterize by the Sahara, the semi-arid and semi-humid zone which move 8°N during January to March to around 15°N at June to August before return in the coastal zone in October to December. The last zone near the equator where the monsoon is permanent with specific humidity of around 15 g kg^{-1}. This migration of the monsoon can be identify the ITCZ fluctuation in Fig. 7 over this region. The maximum vertical motion observed over the Congo basin can be link to the dense forest (also see Fig. 2).

Seasonally averaged values of BLH variance range from 10000 to about 70000 m^2, with mean values around 35000 m^2 (Fig. 8). The year was divided in four periods: January to March (JFM), April to June (AMJ), July to September (JAS), and October to December (OND). In general, JFM and OND correspond to dry season whereas AMJ and JAS correspond to rainy season over West Africa. High values of variance are observed in the tropics close to the ITCZ, where high temperatures and sufficient moisture are available. The high values of variance over west coast of Sahara can be due to the Morocco highland. The root-mean-square error was positive and lees than 0.2 which would indicate a perfect fit to the data. As noted by DeLonge and Fuentes (2012), the unexpected variability observed in the ABL thermodynamic attributes during AMMA campaigns can partly be attributed to the presence of dust layers. Even in the rainy season, dry and dusty air is transported from the Sahara to the West African coast. Impacts of the SAL are often enhanced during periods (AMJ and JAS) with a strong Africa Easterly Jet (AEJ).

The magnitudes of BLH trends are displayed in the Fig. 9 when the level of significance exceeds 95% for the time series (1979 - 2014). Significant trends in BLH occur in the dry Sahara region over Tropical Africa. Regions with a positive trend outnumber the regions of negative trends with magnitudes varying in the time periods considered. Trend magnitudes vary between -20 to 20 m per decade during the period 1979 - 2014. The change of sign yields in a net decrease during 36 years from the dry period (OND and JFM) to the wet season (AMJ and JAS) in the band of latitudes 10°N around Chad and Niger can be due to the migration of the ITCZ which is also linked to the southward decrease of convective available potential energy (CAPE) during the both periods. A similar result on the seasonal study of CAPE trends was found by Meukaleuni et al. (2016).

3.2 Diurnal Cycle of the Atmospheric Boundary Layer Height

Figure 10 presents the vertical variation of wind and virtual potential temperature in the boundary layer at (a) 0000, (b) 0600, (c) 1200, and (d) 1800 UTC in August 2006. Between 10°W and 10°E, the lower BL appear around 875 hPa in the monsoon layer. Wind decreases at the midday (Figs. 10c - d) when the virtual potential temperature [about 300K at 0000 UTC (Fig. 10a)] grows to 310 K at 1800 UTC (Fig. 10d) where the fluctuation of θv is about 10 K. Therefore, on the days with the strongest counter-flow, the SAL contributed to observed ABL features such as strong (> 5 K) capping inversions. When studying the case of 24 August, Jenkins et al. (2010) exhibited the strongest counter-flow, which was also part of the largest SAL event during NASA part of AMMA (NAMMA). The largest capping inversions reported in the present study (Fig. 10) and by others (e.g., Haywood et al. 2003) occurred during SAL events and were associated with sharp differences between the warm, dry desert air aloft ($\theta v \approx 313$ K) and the cooler moister ($\theta v \approx$ 304 K) oceanic counter-flow below. Lapse rates exceeding 6.5 K km^{-1} above the mixed layer were also observed within these dry, dusty air layers.

4. CONCLUSION

A BLH was presented in terms of monthly means, seasonal variances, and trends based on 36 years (1979 - 2014) of six-hourly ERA-Interim reanalysis to characterize and understand the various climate mechanisms that culminate in daily weather over West Africa. The monthly means of BLH show that the influence of the Saharan Air Layer on the BLH and also the impact of monsoon. It was found that the dry region of SAL corresponds to high values of BLH over West Africa from February to October, low values are between Equators to the end of the front of monsoon (around

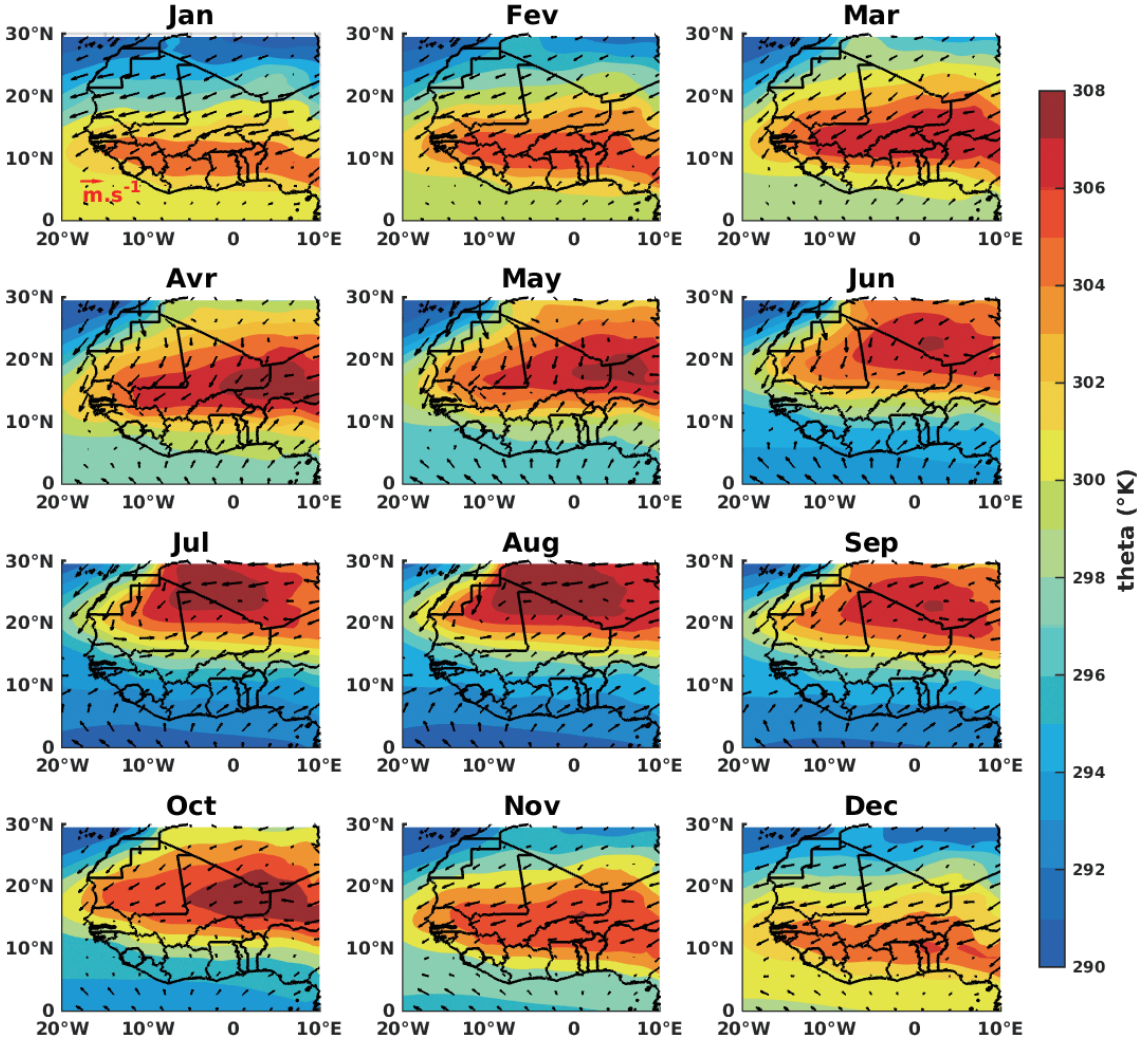

Fig. 5. Climatological (1979 - 2014) monthly means of the potential temperature (θ in K) and 950 hPa wind over West Africa. θ is in the color interval of 2 K whereas the wind vector in arrow as indicated by the legend.

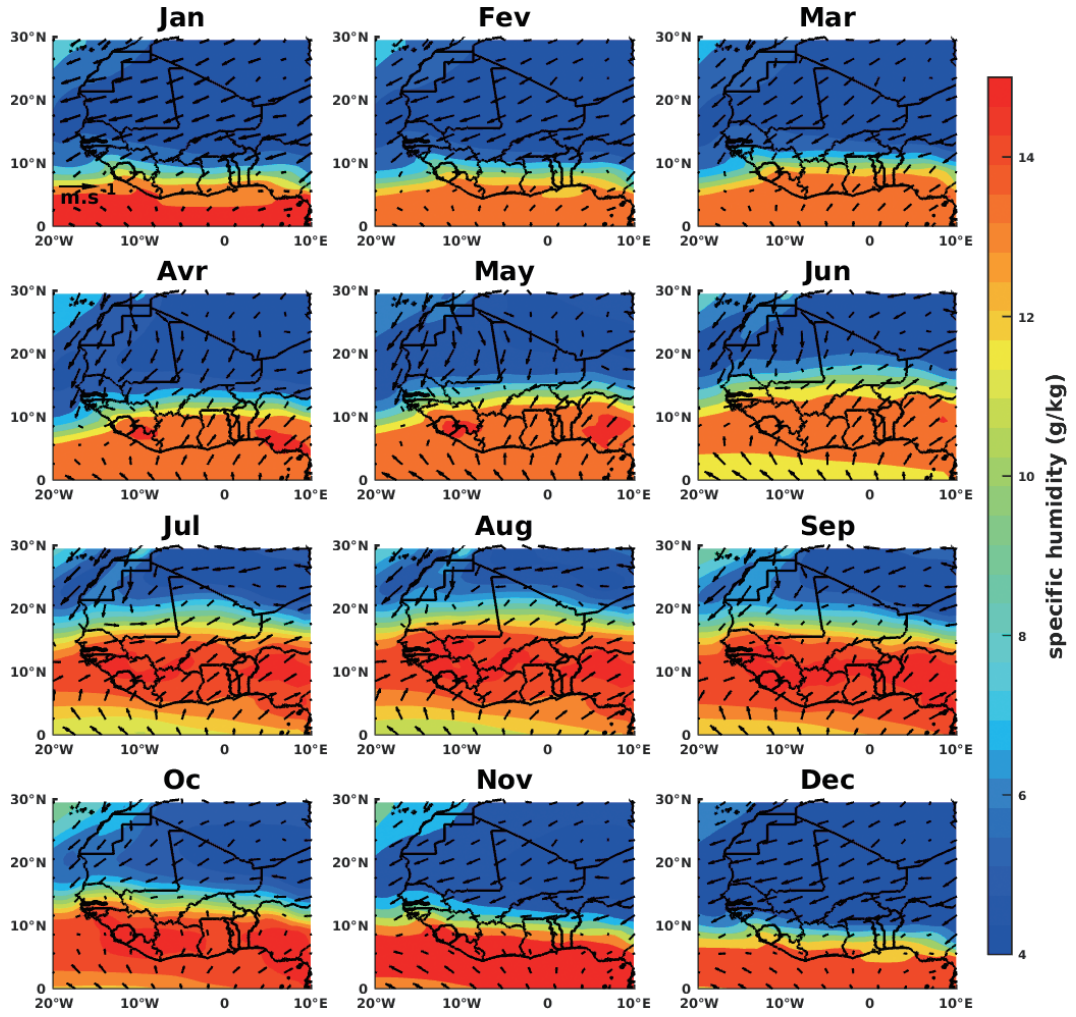

Fig. 6. Climatological (1979 - 2014) monthly means of the specific humidity (Sh in g kg^{-1}) and 950 hPa wind over West Africa. Sh is in the color interval of 2 g kg^{-1} whereas the wind vector in arrow as indicated by the legend.

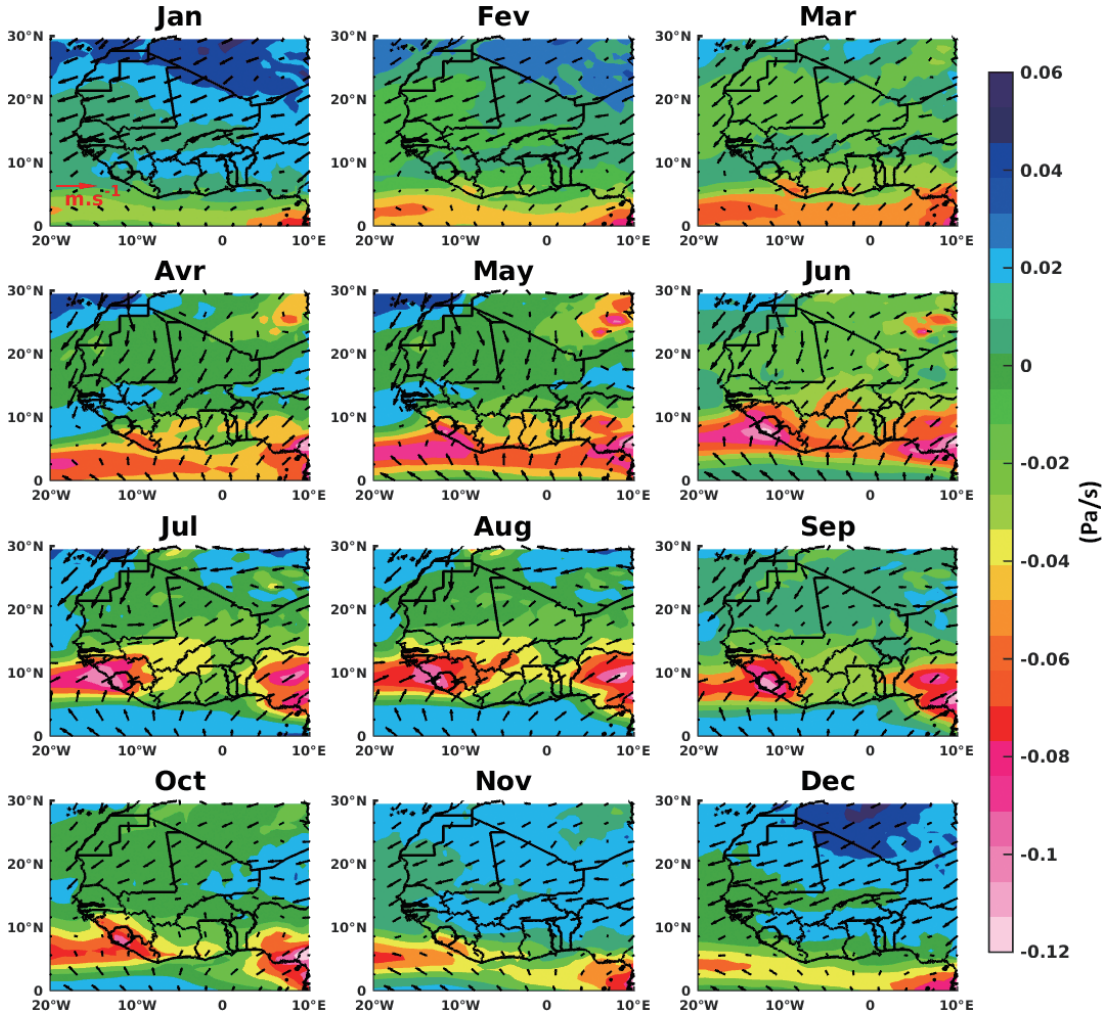

Fig. 7. Climatological (1979 - 2014) monthly means of the vertical motion (ω in Pa s^{-1}) and 500 hPa wind over West Africa. ω is in the color interval of 0.02 Pa s^{-1} whereas the wind vector in arrow as indicated by the legend.

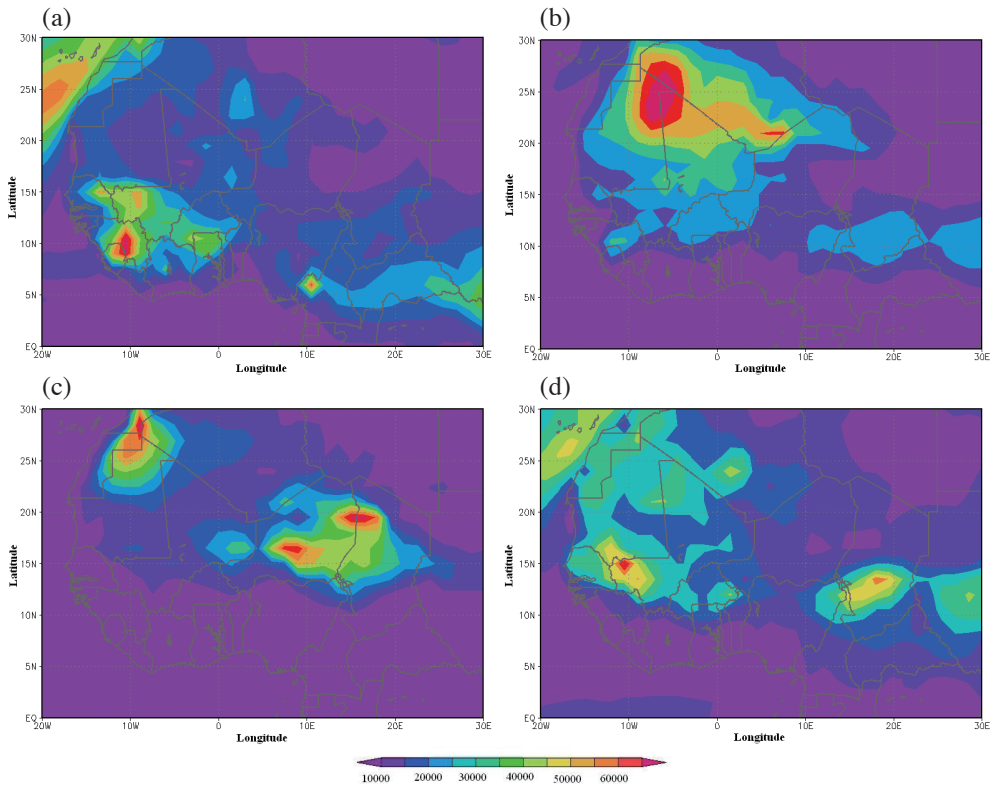

Fig. 8. Climatological (1979 - 2014) inter annual variance of the seasonal BLH in m^2, local averaged during (a) JFM, (b) AMJ, (c) JAS, and (d) OND over West Africa.

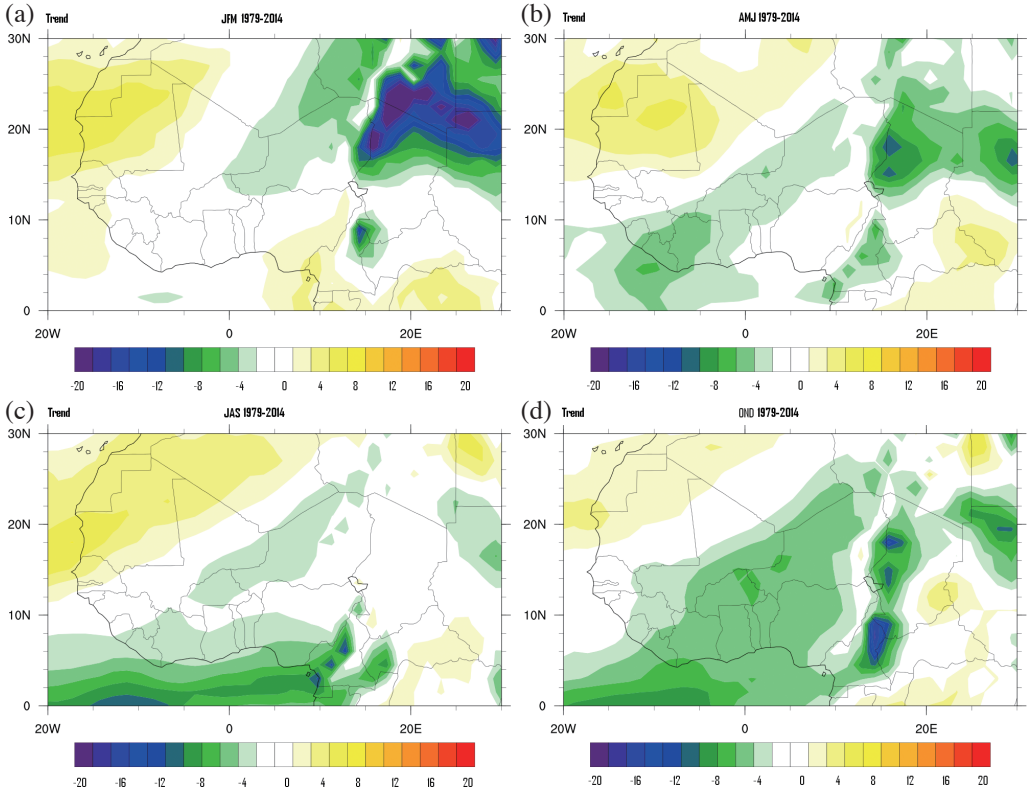

Fig. 9. Seasonal trends of BLH (in meter per decade), significant at the 95% level of JFM, AMJ, JAS, and OND during 1979 - 2014 over West Africa.

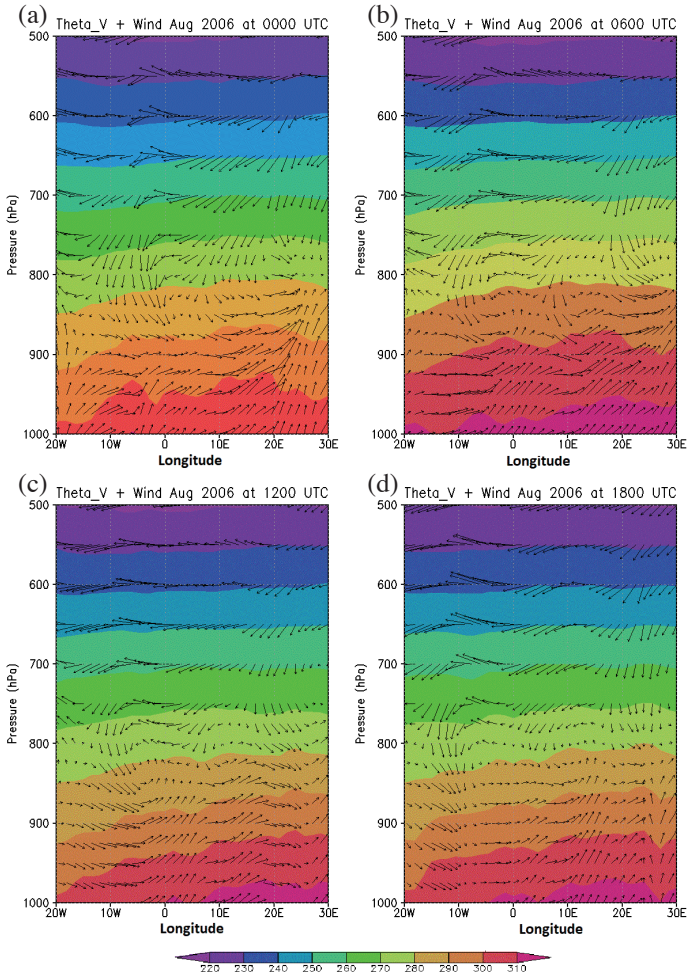

Fig. 10. Vertical and zonal variation of August 2006 diurnal virtual potential temperature (in color interval of 10 K) and wind averaged between 10° - 20°N from the ECMWF Interim Reanalysis at 0000, 0600, 1200, 1800 UTC.

15°) during the summer period (June to September). The monthly variation of Inter Topical Convergent Zone (ITCZ) evolves all during the year between dry and wet region over this region was also noted. Largest values BLH variances were developed in the tropics close to the ITCZ, where high temperatures and sufficient moisture are available. Significant trends in BLH occur in the dry Sahara region over West Africa. For a numerical weather prediction system, BLH can be considered as an output variable to highlight problems in the energy and momentum exchange between the surface and the atmosphere (Caporaso et al. 2013).

Diurnal variation of wind, virtual potential temperature in the boundary layer were analysed during August 2006. The lower BL appear around 875 hPa in the monsoon layer where the wind decreases at the midday when the virtual potential temperature grows.

The data sets produced for this analysis are available as auxiliary material, and in further studies, they can be compared to climate models data sets and their correlation with other atmospheric parameters will be useful.

Acknowledgements The authors thank the Abdus Salam ICTP through the grant OEA-VS506 for funding the stay in Dakar of one of them (AL). They are also grateful to the ECMWF for making their Era-Interim product available to them.

REFERENCES

Adler, R. F., G. J. Huffman, A. Chang, R. Ferraro, P.-P. Xie, J. Janowiak, B. Rudolf, U. Schneider, S. Curtis, D. Bolvin, A. Gruber, J. Susskind, P. Arkin, and E. Nelkin, 2003: The version-2 Global Precipitation Climatology Project (GPCP) Monthly Precipitation Analysis (1979–Present). *J. Hydrometeorol.*, **4**, 1147-1167, doi: 10.1175/1525-7541(2003)004<1147:TVGPCP>2.0.CO;2. [Link]

Ao, C. O., G. A. Hajj, T. K. Meehan, D. Dong, B. A. Iijima, A. J. Mannucci, and E. R. Kursinski, 2009: Rising and setting GPS occultations by use of open-loop tracking. *J. Geophys. Res.*, **114**, D04101, doi:

10.1029/2008jd010483. [Link]

Basha, G. and M. V. Ratnam, 2009: Identification of atmospheric boundary layer height over a tropical station using high-resolution radiosonde refractivity profiles: Comparison with GPS radio occultation measurements. *J. Geophys. Res.*, **114**, D16101, doi: 10.1029/2008JD011692. [Link]

Bolton, D., 1980: The Computation of Equivalent Potential Temperature. *Mon. Weather Rev.*, **108**, 1046-1053, doi: 10.1175/1520-0493(1980)108<1046:TCOEPT>2.0.CO;2. [Link]

Bradley, R. S., F. T. Keimig, and H. F. Diaz, 1993: Recent changes in the North American Arctic boundary layer in winter. *J. Geophys. Res.*, **98**, 8851-8858, doi: 10.1029/93jd00311. [Link]

Caporaso, L., A. Riccio, F. Di Giuseppe, and F. Tampieri, 2013: Relating Mean Radiosounding Profiles to Surface Fluxes for the Very Stable Boundary Layer. *Bound.-Layer Meteor.*, **147**, 203-215, doi: 10.1007/s10546-012-9788-4. [Link]

Carlson, T. N. and J. M. Prospero, 1972: The large-scale movement of Saharan air outbreaks over the Northern Equatorial Atlantic. *J. Appl. Meteorol.*, **11**, 283-297, doi: 10.1175/1520-0450(1972)011<0283:TLSMOS>2.0.CO;2. [Link]

Dee, D. P., S. M. Uppala, A. J. Simmons, P. Berrisford, P. Poli, S. Kobayashi, U. Andrae, M. A. Balmaseda, G. Balsamo, P. Bauer, P. Bechtold, A. C. M. Beljaars, L. van de Berg, J. Bidlot, N. Bormann, C. Delsol, R. Dragani, M. Fuentes, A. J. Geer, L. Haimberger, S. B. Healy, H. Hersbach, E. V. Hólm, L. Isaksen, P. Kållberg, M. Köhler, M. Matricardi, A. P. McNally, B. M. Monge-Sanz, J.-J. Morcrette, B.-K. Park, C. Peubey, P. de Rosnay, C. Tavolato, J.-N. Thépaut, and F. Vitart, 2011: The ERA-Interim reanalysis: Configuration and performance of the data assimilation system. *Q. J. R. Meteorol. Soc.*, **137**, 553-597, doi: 10.1002/qj.828. [Link]

DeLonge, M. and J. D. Fuentes, 2012: Controls on Boundary-Layer Thermodynamics and Dynamics in Coastal West Africa during the Rainy Season of 2006. *Bound.-Layer Meteor.*, **145**, 113-130, doi: 10.1007/s10546-012-9734-5. [Link]

Dunion, J. P. and C. S. Velden, 2004: The impact of the Saharan Air Layer on Atlantic tropical cyclone activity. *Bull. Amer. Meteorol. Soc.*, **85**, 353-366, doi: 10.1175/bams-85-3-353. [Link]

Farquharson, J. S., 1939: The diurnal variation of wind over tropical Africa. *Q. J. R. Meteorol. Soc.*, **65**, 165-184, doi: 10.1002/qj.49706528004. [Link]

Flamant, C., J.-P. Chaboureau, D. J. Parker, C. M. Taylor, J.-P. Cammas, O. Bock, F. Timouk, and J. Pelon, 2007: Airborne observations of the impact of a convective system on the planetary boundary layer thermodynamics and aerosol distribution in the inter-tropical discontinuity region of the West African Monsoon. *Q. J. R. Meteorol. Soc.*, **133**, 1175-1189, doi: 10.1002/qj.97. [Link]

Garratt, J. R., 1992: The Atmospheric Boundary Layer, Cambridge University Press, 334 pp.

Haywood, J., P. Francis, S. Osborne, M. Glew, N. Loeb, E. Highwood, D. Tanré, G. Myhre, P. Formenti, and E. Hirst, 2003: Radiative properties and direct radiative effect of Saharan dust measured by the C-130 aircraft during SHADE: 1. Solar spectrum. *J. Geophys. Res.*, **108**, doi: 10.1029/2002JD002687. [Link]

Holzworth, G. C., 1964: Estimates of mean maximum mixing depths in the contiguous United States. *Mon. Weather Rev.*, **92**, 235-242, doi: 10.1175/1520-0493(1964)092<0235:EOMMMD>2.3.CO;2. [Link]

Huffman, G. J., R. F. Adler, M. M. Morrissey, D. T. Bolvin, S. Curtis, R. Joyce, B. McGavock, and J. Susskind, 2001: Global Precipitation at One-Degree Daily Resolution from Multisatellite Observations. *J. Hydrometeorol.*, **2**, 36-50, doi: 10.1175/1525-7541(2001)002<0036:GPAODD>2.0.CO;2. [Link]

Jenkins, G., P. Kucera, E. Joseph, J. Fuentes, A. Gaye, J. Gerlach, F. Roux, N. Viltard, M. Papazzoni, A. Protat, D. Bouniol, A. Reynolds, J. Arnault, D. Badiane, F. Kebe, M. Camara, S. Sall, S. A. Ndiaye, and A. Deme, 2010: Coastal observations of weather features in Senegal during the African Monsoon Multidisciplinary Analysis Special Observing Period 3. *J. Geophys. Res.*, **115**, D18108, doi: 10.1029/2009JD013022. [Link]

Kang, Y.-H., S.-K. Song, M.-K. Hwang, J.-H. Jeong, and Y.-K. Kim, 2016: Impacts of detailed land-use types and urban heat in an urban canopy model on local meteorology and ozone levels for air quality modeling in a coastal city, Korea. *Terr. Atmos. Ocean. Sci.*, **27**, 877-891, doi: 10.3319/TAO.2016.01.13.01(A). [Link]

Lenouo, A., A. D. Vondou, W. M. Pokam, T. L. A. Djiotang, and F. Mkankam Kamga, 2008: The computation of Equivalent Static Stability Measures. *AJST*, **9**, 60-63.

Meukaleuni, C., A. Lenouo, and D. Monkam, 2016: Climatology of Convective Available Potential Energy (CAPE) in ERA-Interim reanalysis over West Africa. *Atmos. Sci. Lett.*, **17**, 65-70, doi: 10.1002/asl.601. [Link]

Nau, R., 2014: Review of basic statistics and the simplest forecasting model: The sample mean. Fuqua School of Business, Duke University, 18 pp.

Oke, T. R., 1988: Boundary Layer Climates, 2 Edition, The Psychology Press, Routledge, 464 pp.

Parker, D. J., R. R. Burton, A. Diongue-Niang, R. J. Ellis, M. Felton, C. M. Taylor, C. D. Thorncroft, P. Bessemoulin, and A. M. Tompkins, 2005: The diurnal cycle

of the West African monsoon circulation. *Q. J. R. Meteorol. Soc.*, **131**, 2839-2860, doi: 10.1256/qj.04.52. [Link]

Schrage, J. M., S. Augustyn, and A. H. Fink, 2007: Nocturnal stratiform cloudiness during the West African monsoon. *Meteorol. Atmos. Phys.*, **95**, 73-86, doi: 10.1007/s00703-006-0194-7. [Link]

Seibert, P., F. Beyrich, S.-E. Gryning, S. Joffre, A. Rasmussen, and P. Tercier, 2000: Review and intercomparison of operational methods for the determination of the mixing height. *Atmos. Environ.*, **34**, 1001-1027, doi: 10.1016/S1352-2310(99)00349-0. [Link]

Seidel, D. J., C. O. Ao, and K. Li, 2010: Estimating climatological planetary boundary layer heights from radiosonde observations: Comparison of methods and uncertainty analysis. *J. Geophys. Res.*, **115**, D16113, doi: 10.1029/2009JD013680. [Link]

Seidel, D. J., Y. Zhang, A. Beljaars, J.-C. Golaz, A. R. Jacobson, and B. Medeiros, 2012: Climatology of the planetary boundary layer over the continental United States and Europe. *J. Geophys. Res.*, **117**, D17106, doi: 10.1029/2012JD018143. [Link]

Slingo, A., T. P. Ackerman, R. P. Allan, E. I. Kassianov, S. A. McFarlane, G. J. Robinson, J. C. Barnard, M. A. Miller, J. E. Harries, J. E. Russell, and S. Dewitte, 2006: Observations of the impact of a major Saharan dust storm on the atmospheric radiation balance. *Geophys. Res. Lett.*, **33**, L24817, doi: 10.1029/2006GL027869. [Link]

Smith, E. K. and S. Weintraub, 1953: The Constants in the Equation for Atmospheric Refractive Index at Radio Frequencies. *Proceedings of the IRE*, **41**, 1035-1037, doi: 10.1109/JRPROC.1953.274297. [Link]

Sokolovskiy, S., Y.-H. Kuo, C. Rocken, W. S. Schreiner, D. Hunt, and R. A. Anthes, 2006: Monitoring the atmospheric boundary layer by GPS radio occultation signals recorded in the open-loop mode. *Geophys. Res. Lett.*, **33**, L12813, doi: 10.1029/2006GL025955. [Link]

Sorbjan, Z., 1989: Structure of the Atmospheric Boundary Layer, Prentice Hall, New Jersy, 317 pp.

Stull, R. B., 1988: An Introduction to Boundary Layer Meteorology, Springer, Dordrecht, 670 pp, doi: 10.1007/978-94-009-3027-8. [Link]

Troen, I. B. and L. Mahrt, 1986: A simple model of the atmospheric boundary layer; Sensitivity to surface evaporation. *Bound.-Layer Meteor.*, **37**, 129-148, doi: 10.1007/BF00122760. [Link]

Xie, P., J. E. Janowiak, P. A. Arkin, R. Adler, A. Gruber, R. Ferraro, G. J. Huffman, and S. Curtis, 2003: GPCP Pentad Precipitation Analyses: An Experimental Dataset Based on Gauge Observations and Satellite Estimates. *J. Clim.*, **16**, 2197-2214, doi: 10.1175/2769.1. [Link]

Xu, H., G. Zhai, D. Wang, H. Shen, and R. Liu, 2015: An evaluation of the Mellor-Yamada-Janjić formulation parameters for the QNSE scheme in the WRF Model over the Lower Yangtze River valley. *Terr. Atmos. Ocean. Sci.*, **26**, 283-299, doi: 10.3319/TAO.2014.11.24.01(A). [Link]